Multiple Determinants and Consequences of Cohesion Fatigue in Mammalian Cells

Hem Sapkota[1,2], Emilia Wasiak[2] and Gary J. Gorbsky[2,3]

1. Department of Cell Biology, University of Oklahoma Health Sciences Center, Oklahoma City, OK 73104, USA
2. Cell Cycle and Cancer Biology Research Program, Oklahoma Medical Research Foundation, Oklahoma City, OK 73104, USA
3. Corresponding author

Condensed Title: Determinants and consequences of cohesion fatigue

Abstract

Cells delayed in metaphase with intact mitotic spindles undergo cohesion fatigue, where sister chromatids separate asynchronously, while cells remain in M phase. Cohesion fatigue requires release of sister chromatid cohesion. However, the pathways necessary to breach sister chromatid cohesion during cohesion fatigue remain unknown. Using a regulated protein heterodimerization system to lock different cohesin interfaces at specific times in mitosis, we show that the prophase pathway of Cohesin release is not required for cohesion fatigue. By manipulating microtubule stability and Cohesin complex integrity in cell lines with varying sensitivity to cohesion fatigue, we show that rates of cohesion fatigue reflect a dynamic balance between spindle pulling forces and resistance to separation by interchromatid cohesion. Cohesion fatigue that results in complete chromatid separation may be an unrecognized but common source of chromosome instability. Here, we extend the significance of cohesion fatigue by showing that even limited delays at metaphase lead to partial centromere separation and predispose cells to chromosome missegregation.

Introduction:

Cells delayed or arrested at metaphase with intact mitotic spindles undergo cohesion fatigue, where sister chromatids separate asynchronously, while the cells remain in M phase (Daum et al., 2011; Stevens et al., 2011). Separated chromatids generated before anaphase likely missegregate or form merotelic attachments that can result in aneuploidy and chromosome breakage. While all cells can undergo cohesion fatigue when arrested at metaphase, the rate of chromatid separation varies significantly within a population of cells and among different cell lines, even those closely related.

The Cohesin complex normally holds sister chromatids together from DNA replication until anaphase (Michaelis et al., 1997). The major structural elements of the Cohesin ring consists of two Structural Maintenance of Chromosome proteins (SMC3 and SMC1) and cohesin complex component RAD21 that closes the ring. These proteins intersect at three sites, referred to as “gates.” Cohesin gates may open during different stages of dynamic Cohesin-chromatin interactions during the cell cycle. For example, Cohesin appears to load onto chromosomes via the opening of the SMC3 and SMC1 hinge interface (Buheitel and Stemmann, 2013) and partially through the SMC3 and RAD21 interface (Murayama and Uhlmann, 2015). To release sister chromatids from each other in mitosis in vertebrates, Cohesin complexes are removed from chromosomes through two mechanisms. In early mitosis until metaphase, the prophase pathway uses Plk1 and Aurora B kinases and the Cohesin removal protein, Wapl, to release a large portion of Cohesin from chromosome arms. Then at the metaphase-anaphase transition, the protease, Separase, cleaves the RAD21 component of the remaining chromosome-bound Cohesin to induce the final separation of sister chromatids (Waizenegger et al., 2000).

In addition to its three core structural ring components, the Cohesin complex contains several regulatory auxiliary components. One has two isoforms called Stromal Antigen 1 and 2

(SA1 or SA2) (Solomon et al., 2011; Sumara et al., 2000). Cohesin complexes contain either SA1 or SA2 (Zhang et al., 2008). Cells depleted of one can continue to proliferate, but deletion of both is lethal (van der Lelij et al., 2017). Cohesin complexes containing SA1 appear important for arm and telomere cohesion, while Cohesin complexes containing SA2 have more critical roles for centromeric cohesion (Canudas and Smith, 2009). SA2 at centromeres recruits proteins that promote cohesion, including Sororin, Shugoshin (SGO1), and Protein Phosphatase 2A (PP2A), that shield centromeric Cohesin from phosphorylation and removal due to the prophase pathway (Hauf et al., 2005; McGuinness et al., 2005; Nishiyama et al., 2013).

The separation of chromatids in cohesion fatigue requires release of sister chromatid cohesion. However, we do not know if and how the Cohesin complex is breached during cohesion fatigue. Although we and others have shown that depletion of Wapl, a negative regulator of cohesin, prior to mitotic entry, delays cohesion fatigue, it is still unclear whether Wapl plays an active role during fatigue. Previously, we reported that Cohesin protein levels in chromosome fractions remained constant before and after cohesion fatigue (Daum et al., 2011). However, a subsequent study indicated that most Cohesin bound to isolated chromosomes could be salt-extracted, raising the possibility that only the salt-resistant Cohesin is functional in holding sister chromatids together (Bermudez et al., 2012). Cohesion fatigue may generate partially separated chromatids at metaphase. These defects may not be detected and resolved. Thus, it is unclear if and how various degrees of cohesion fatigue promote genomic instability.

Currently, we do not comprehensively understand the factors that determine the sensitivity of a cell to cohesion fatigue. Microtubule pulling forces are essential. Treatment of cells with Nocodazole, a microtubule depolymerizer, completely eliminates cohesion fatigue in mitotic cells arrested by treatment with the proteasome inhibitor, MG132, or by depletion of the SKA3 protein (Daum et al., 2011). In normal mitosis at metaphase, the pulling forces of kinetochore interactions with spindle microtubules are counterbalanced by sister chromatid cohesion

mediated by the Cohesin complex. To map the relative contributions of various determinants, we manipulated spindle microtubule dynamics and Cohesin components and regulators. We show that experimentally stabilizing or destabilizing spindle microtubules can increase or decrease the rate of cohesion fatigue, respectively. Compromising Cohesin integrity also accelerates fatigue. We also examined the fate of the major structural, salt-resistant, Cohesin proteins but found little difference in the chromatid-bound fraction before or after fatigue. In addition, we artificially locked different protein-protein interfaces of the Cohesin ring during different stages of mitosis to delineate whether the prophase pathway gate was actively breached during cohesion fatigue. Surprisingly we discovered that neither the prophase-pathway-gate, nor any other gates, are breached in cohesion fatigue. Acute inhibition of prophase pathway during metaphase arrest has no effect on timing of cohesion fatigue, suggesting prophase pathway is dispensable for cohesion fatigue. Massive scale cohesion fatigue, where many chromosomes separate before anaphase onset, likely generates inviable cell progeny. More subtle and perhaps more insidious chromosome instabilities might arise after partial separation of chromatids and/or complete separation of just one or a few chromosomes. To test chromosome instability after partial separation or limited chromatid separation, we analyzed the consequences of shorter delays at metaphase and determined that transient delays can predispose cells to chromosome missegregation.

Results:

Perturbing microtubule stability alters the rate of cohesion fatigue.

For our studies, we used two isolates of HeLa cells that exhibit differences in the rate of cohesion fatigue (Supplementary figures 1A and 1B). One HeLa cell line, stably expressing histone H2B-GFP, undergoes cohesion fatigue with an average time of approximately 340±127

min at metaphase, while another HeLa cell line, stably expressing histone H2B-mRFP, undergoes cohesion fatigue after an average of 130±55 min. We named these cell lines HeLa-Slow and HeLa-Fast, respectively. We induced metaphase arrest by treating cells with ProTAME, a cell permeant inhibitor of the Anaphase Promoting Complex/Cyclosome (APC/C) (Lara-Gonzalez and Taylor, 2012; Sackton et al., 2014) or MG132, a proteasome inhibitor.

We had previously shown that disruption of spindle microtubules completely blocked cohesion fatigue, which indicated that spindle pulling forces were essential (Daum et al, 2011). However, it was unclear how modulating these pulling forces by changing normal microtubule dynamics might affect cohesion fatigue efficiency. To alter microtubule dynamics while leaving spindles intact, we used 5 nM Nocodazole and 1.5 nM Taxol, concentrations that slow but do not block progression of control cells through mitosis (Supplementary figure 1C). We measured the elapsed time from metaphase to chromosome scattering (fatigue) in cells arrested at metaphase. Treatment with 5 nM Nocodazole to partially destabilize microtubules marginally delayed chromosome alignment, but significantly slowed cohesion fatigue in both HeLa-Slow and HeLa-Fast cells (Figures 1A and 1B). Correspondingly, partial stabilization of spindle microtubules with 1.5 nM Taxol led to faster cohesion fatigue in both cell types (Figures 1C and 1D). When taken as percentage, HeLa-Slow and HeLa-Fast cells showed comparable delays in cohesion fatigue when treated with Nocodazole and comparable acceleration when treated with Taxol.

We also treated cells with low concentrations of S-Trityl-L-cysteine (STLC), an inhibitor of mitotic motor kinesin Eg5 (Skoufias et al., 2006). At high concentrations, STLC induces collapse of spindle poles. But, at reduced concentrations, spindles can be maintained with decreased interpolar distance and diminished spindle tension (Vallot et al., 2017). The decrease in spindle tension would be expected to reduce the outward force on kinetochores. In control cells, 1.5 uM STLC caused only slight delay in normal mitotic progression (Supplementary figure

1D). In cells arrested at metaphase, STLC treatment led to significantly slower cohesion fatigue in both HeLa-Slow and HeLa-Fast cells (Figures 1E and 1F).

Compromised Cohesin accelerates cohesion fatigue.

Cohesin-chromatin interactions are highly regulated throughout cell cycle (Bermudez et al., 2012; Gandhi et al., 2006; Lara-Gonzalez and Taylor, 2012; Liu et al., 2013a; Whelan et al., 2012; Xu et al., 2014). In early mitosis, Cohesin is removed from chromosome arms by the prophase pathway through mitotic kinases and the Cohesin release protein, Wapl (Gandhi et al., 2006; Kueng et al.; Nishiyama et al., 2010; Nishiyama et al., 2013; Shintomi and Hirano, 2009). In cells arrested in mitosis for long periods, Cohesin removal separates chromosome arms, which generates the classic “X-shape” chromosomes seen in chromosome spreads (Supplementary figure 2A). We previously found that under normal conditions, cohesion fatigue initiates at kinetochores then propagates down the chromosome arms. Thus, Cohesin loss and arm separation should increase cell susceptibility to cohesion fatigue. To test this idea, we used chromosome spreads to compare rates of cohesion fatigue in LLC-PK cells after arresting cells in mitosis for 5 or 11 h with Nocodazole. After Nocodazole arrest, cells were washed then placed in fresh media containing MG132 and then processed for chromosome spreads immediately (0 h), 3 h or 6 h later (Figure 2A). Cells arrested in Nocodazole for 11 h had significantly increased cohesion fatigue compared to cells arrested for just 5 h (Figure 2B). In contrast, cells harvested at 0 h, 3 h or 6 h after being maintained in MG132 plus Nocodazole showed very few separated chromatids. We hypothesized that arrest in Nocodazole might decrease the level of Cohesin on chromosomes. Quantification of western blots showed a modest decrease in chromosome-bound Cohesin levels between 5 and 11 h (Supplementary figure 2C). These results indicate that longer mitotic arrest, without spindle pulling forces, primes cells to undergo faster cohesion fatigue.

These results indicated that the increased time spent in mitosis led to higher propensity for cohesion fatigue. As a complimentary method to test this idea, we compared onset of cohesion fatigue in cells that reach full metaphase quickly with those delayed in chromosome alignment. To increase the proportion of cells with alignment delays, we treated cells with a 1.5 uM concentration of the Eg5 inhibitor, STLC. When we measured the time from full metaphase alignment to cohesion fatigue, cells with the slowest alignment, and thus with longer times spent in prometaphase, showed faster rates of cohesion fatigue (Supplementary figure 2B).

As noted, the Cohesin subunit SA2 is thought to promote centromere cohesion. Unlike Sgo1 depletion where sister chromatids separate without any spindle force, depletion of SA2 causes increased interkinetochore distance only in the presence of spindle force (Kleyman et al., 2014) suggesting defective cohesion maintenance rather than compromised cohesion establishment. If so, then depletion of SA2 should accelerate cohesion fatigue. We investigated the consequences of SA2 loss using HCT116 cells in which the STAG2 gene, which codes for SA2, had been deleted by homologous recombination (Solomon et al., 2011). Chromosomes from SA2 knockout cells showed reduced amounts of the Cohesin ring components, SMC3 and RAD21, compared to parental HCT116 cells (Supplementary figure 2E). Metaphase arrest for 3 or 6 h caused increased separation of chromatids in chromosome spreads of SA2 knockout cells compared to parental cells (Figure 2C). Inclusion of nocodazole to disrupt spindle microtubules abrogated the differences in chromatid separation in SA2 knockout and parental cells. Thus, loss of the Cohesin regulatory component, SA2, increases the susceptibility of cells to cohesion fatigue in the presence of spindle pulling forces. Because SA2 helps to resist cohesion fatigue, we hypothesized that its release might accompany fatigue. We analyzed chromosome fractions from HeLa cells by western blot before and after fatigue but found no reduction in the amount of chromosome-bound SA2 after chromatid separation (Figure 2D).

Cohesin remains bound to chromatids after fatigue.

The fact that cohesion fatigue can generate separate chromatids (Figure 3A, 3B) suggests that logically Cohesin is released from chromosomes during the process. However, in a previous study comparing isolated chromosomes and chromatids prepared from cells before and after fatigue, we made the surprising discovery that levels of the core Cohesin subunits bound to chromatin were unchanged (Daum et al., 2011). However, much chromatin-associated Cohesin from isolated mitotic chromosomes is loosely bound and is released by treatment of chromosomes with buffer containing moderate amounts of salt (Bermudez et al., 2012). In addition, recent work in Drosophila, where total Cohesin levels were genetically regulated, shows that expression of low levels of Cohesin can maintain normal sister chromatid cohesion at metaphase (Oliviera, personal communication). We hypothesized that perhaps the minor, salt-resistant fraction on isolated mammalian chromosomes may reflect the functional Cohesin that maintains sister chromatid cohesion, so perhaps this portion might be released during cohesion fatigue.

We first confirmed that only a fraction of Cohesin remains bound to chromosomes after treatment with high salt buffer (Supplementary figure 3B). We then examined whether any changes occurred in the salt-resistant population before and after cohesion fatigue. We treated mitotic cells with MG132 in the absence or presence of Nocodazole for 8 h and then isolated chromosome fractions with high salt buffers. As expected, more than 90% of cells treated with MG132 without Nocodazole had separated chromatids compared with only 5% of cells treated with MG132 in the presence of Nocodazole (Figure 3B). We immunoblotted for the core Cohesin component, SMC3, and found no change in salt-resistant Cohesin levels in cells with separated chromatids (Figures 3C and 3D). Thus, we do not detect Cohesin release in either the total chromosome-bound population or the salt-resistant population during cohesion fatigue.

The Shugoshin1 (SGO1) protein protects centromeric Cohesin from the prophase pathway by recruiting protein phosphatase 2A (PP2A) to the centromere region (Gandhi et al., 2006; Liu et al., 2013b; Shintomi and Hirano, 2009; Xu et al., 2009). Changes in SGO1 have been implicated in sensitivity to chromatid separation during metaphase arrest (Liu et al., 2013a; Tanno et al., 2015). We examined how changes in centromere-associated levels of SGO1 accompany cohesion fatigue in our cells. We measured total SGO1 levels in both HeLa-Fast and HeLa-Slow cells and compared SGO1 levels by immunofluorescence in normal prophase, prometaphase or metaphase cells and in cells arrested in metaphase for 6 h (HeLa-Slow) or 3 h (HeLa-Fast). From metaphase-arrested cells, we selected fatigued cells and examined their SGO1 levels. In HeLa-Slow cells, SGO1 levels diminished from prometaphase to metaphase, but no further reduction in SGO1 levels occurred with metaphase arrest for 6 h. Cells with separated chromatids showed no reduction in SGO1 levels compared to normal metaphase-arrested cells (Supplementary figure 3D). HeLa-Fast cells showed a similar trend during mitotic progression with SGO1 showing reduced levels at metaphase. In these cells, SGO1 levels were further decreased after 3 h of metaphase delay. However, in cells that underwent cohesion fatigue during the 3 h metaphase delay, SGO1 levels were equal to levels of normal metaphase cells (Supplementary figure 3E). Thus, both cell lines showed a reduction in centromere-associated SGO1 levels as the cells aligned their chromosomes, but SGO1 did not appear to be altered during fatigue. Finally, comparison of total chromosome associated SGO1 levels showed higher levels in HeLa-Fast cells than in HeLa-Slow cells, the opposite that might be expected if SGO1 levels were a major determinant of resistance to cohesion fatigue (Supplementary figure 3C).

The prophase pathway is not essential for cohesion fatigue

We and others have previously shown that depletion of Wapl, which mediates Cohesin removal through the prophase pathway, delays cohesion fatigue (Daum et al., 2011; Stevens et al., 2011). To extend these studies in a system where enhanced Cohesin binding to mitotic chromosomes could be directly monitored, we used Hela cells stably expressing SMC1-GFP (Hou et al., 2007) and examined the effects of Wapl depletion. We depleted Wapl via RNAi, treated the SMC1-GFP cells with ProTAME, and examined cells with clear SMC1-GFP signals on metaphase chromosomes, indicative of those with efficient Wapl depletion (Supplementary figure 4A). Normally, Cohesin released into the cytoplasm by the prophase pathway obscures the residual chromosome-bound population, but Wapl depletion results in strong retention of chromosome Cohesin (Gandhi et al., 2006; Haarhuis et al., 2013; Haarhuis et al., 2017; Tedeschi et al., 2013). When Wapl-depleted cells were arrested at metaphase, there was a significant increase in time these cells take to undergo cohesion fatigue (Figure 4A), confirming that Wapl depletion causes increased chromosome association of Cohesin and delayed cohesion fatigue without affecting the total number of cells undergoing fatigue. To extend the Wapl depletion studies, we examined, Sororin, a key upstream player in prophase pathway. We tested whether expression of non-phosphorylatable Sororin mutant (9A-Sororin), which is shown to inhibit prophase pathway, could delay cohesion fatigue (Liu et al., 2013b). Similar to Wapl depletion, cells expressing the 9A mutant form of Sororin showed significant delay in cohesion fatigue compared to WT controls (Figure 4B).

The above studies show that inhibiting the prophase pathway slows cohesion fatigue. This might occur through two mechanisms. First, inhibition of Wapl function in the prophase pathway might simply result in greater levels of cohesive Cohesin retained on chromosomes. Second, Wapl may functionally participate in opening Cohesin rings during cohesion fatigue. These two mechanisms are not mutually exclusive. Two mitotic kinases, Plk1 and Aurora B are critical for the function of the prophase pathway. In our previous work, we showed that chemical

inhibition of Plk1 did not block cohesion fatigue in the HeLa-Slow cell line, but in that study, the rates of fatigue were not quantified (Daum et al., 2011). Here we used 2.5 µM ZM447439, an inhibitor of Aurora B kinase to inhibit the prophase pathway in HeLa-Slow cells. Treatment of cells in early mitosis with 0.5 µM ZM447439, a 5-fold lower concentration, caused significant defects in chromosome alignment, confirming inhibition of Aurora B kinase (Supplementary figure 4B). By adding the inhibitor after most cells had aligned their chromosomes, one hour after release from nocodazole to MG132, we avoided affecting chromosome alignment. Then we analyzed the cells that had tight metaphase plates at the time of ZM447439 addition. Addition of 2.5 µM ZM447439 did not cause noticeable alteration in alignment of chromosomes at metaphase. The Aurora B inhibitor did not cause a delay in cohesion fatigue suggesting that the continued activity of the prophase in cells arrested at metaphase does not contribute to cohesion fatigue in these cells (Figure 4C).

The Wapl-mediated prophase pathway releases Cohesin by opening the SMC33-RAD21 interface or gate. As a stringent test of the role of the prophase pathway in cohesion fatigue we used three HEK293 cells lines, each expressing a pair of Cohesin ring components tagged with FRB or FKBP proteins that allows locking of SMC3-RAD21 gate, the SMC1-RAD21 gate, and the SMC1-SMC3 gate by the addition of Rapamycin (Buheitel and Stemmann, 2013). We depleted endogenous Cohesin proteins and induced expression of the siRNA-resistant fusion proteins. We used chromosome spreads to confirm previously published work that locking the SMC3-RAD21 gate, but not the other gates, inhibited prophase pathway-mediated release of Cohesin and increased the proportion of chromosomes with unresolved chromosome arms (Supplementary figures 4C and 4D). We then studied the effect on cohesion fatigue (Figure 4E). As expected, when we locked the gates before cells entered mitosis, chromosome spreads showed that cohesion fatigue was inhibited only in cells expressing the SMC3-RAD21 pair of Rapamycin binding proteins, mimicking Wapl depletion (Figure 4F). The other two lines were

unaffected. These results were confirmed by live cell imaging (Supplementary figure 4E). These data showed that gate locking was efficient, that locking only the SMC3-RAD21 gate mimicked Wapl depletion in blocking the prophase pathway, and that Rapamycin-induced dimerization of SMC3-RAD21 could resist spindle-pulling forces. Next, we locked the Cohesin gates after completion of the prophase pathway by adding Rapamycin to cells after they entered mitosis (Figure 4E; after +/- Rapa). Consistent with our results from Aurora B inhibition, chromosome spreads showed that abrogation of the prophase pathway after metaphase alignment did not inhibit cohesion fatigue (Figure 4G). These results indicate that inhibition of the prophase pathway early in mitosis can delay cohesion fatigue, likely through an increase in the amount of functional Cohesin retained on chromosomes. However, once cells are at metaphase, inhibition of the Wapl-mediated prophase pathway does not delay fatigue, indicating it is not required for chromatid separation. In addition, locking the other Cohesin gates does not affect fatigue. Thus, transient opening of a single Cohesin gate is unlikely to account for the separation of sister chromatids in cohesion fatigue for the cells we have analyzed.

Short delays at metaphase induce partial separation of chromatids at their kinetochores.

Chromatid separation in cohesion fatigue is progressive, initiating at the kinetochores then advancing distally along the chromosome arms (Daum et al., 2011). To evaluate the time-course of chromatid separation after short delays, we tracked the interkinetochore distance between sister chromatids in LLC-PK cells. We detected significant separation of kinetochores in cells treated with MG132 for 3 h (Figures 5A and B). In most cells arrested for 3 h, sister chromatid arms remained attached, but kinetochores were significantly separated with many showing separations of more than 3 µm versus 1.75 µm in control metaphase cells and 0.7 µm in cells treated with 330 nM nocodazole (Figure 5C and Supplementary figure 5A). Like LLC-PK cells, HeLa cells also showed increased interkinetochore distances when delayed at metaphase for 3 h (Supplementary figure 5B). To examine the dynamics of chromatid separation in detail,

we used live cell imaging to monitor metaphase-arrested LLC-PK cells expressing GFP-Topoisomerase IIα, which highlights both kinetochores and chromosome arms. Cells treated with MG132 for 3 h showed a significantly larger range of interkinetochore stretching compared to those treated for only 1 h. In control metaphase and 1 h metaphase-arrested cells, the average interkinetochore distance varied approximately 0.4 μm as sister kinetochores oscillated together and apart. In contrast, cells arrested at metaphase for 3 h showed stretching between sister kinetochores of 1 μm or more (Figure 5D). Similar to the fixed cells analysis, a 3 h delay at metaphase also generated longer average distances between kinetochore pairs compared to control metaphase (Supplementary figure 5C). Overall, moderate delays at metaphase cause abnormal separation of kinetochores.

Partial separation of chromatids induces segregation defects.

Transient delays during late prometaphase with most chromosomes at the metaphase plate are common during unperturbed mitosis, which often occurs as one or more chromosomes lag in their congression to the spindle midline. To examine the immediate impact of partial chromatid separation that may occur during a transient delay, we arrested cells at metaphase, then released them into anaphase. We arrested LLC-PK cells with 5 μM MG132 for 3 h. Cells were washed into fresh medium without drug and then fixed 3.5 h later when most had entered anaphase. We examined every cell that entered anaphase for lagging chromosomes, anaphase bridges or micronuclei (Figure 6A). Cells arrested at metaphase for 3 h with MG132 treatment exited mitosis with an error rate of ~44%. Untreated control cells exited mitosis with a missegregation rate of ~4%. Cells treated and released from a 3 h Nocodazole arrest exhibited a slightly elevated error rate of 7%. Cells treated and released after a treatment with both MG132 and Nocodazole showed segregation errors in 18% of anaphases, significantly lower than MG132 treatment alone (Figure 6B). Because mitotic exit after release from MG132 requires approximately 3.5 h and recovery from Nocodazole takes only 30-60 min, cells

released from the combination of MG132 and Nocodazole become arrested at metaphase with an intact spindle for approximately 3 h. This finding is consistent with the higher rate of anaphase defects in these cells compared with controls. We also compared the accumulation of segregation defects in cells arrested at metaphase for different durations. We treated LLC-PK cells with MG132 for 1 or 4 h, released them in fresh medium and then evaluated the anaphases. In cells arrested for 1 h, only 13% of the anaphases showed segregation errors, while 55% of cells arrested for 4 h revealed errors (Supplementary figure 6A).

Non-cancer cells that missegregate chromosomes generally arrest in the next interphase through a p53-dependent mechanism (Thompson and Compton, 2010). Not all anaphase chromosome segregation errors cause aneuploidy, as some defects such as lagging chromosomes are properly incorporated into daughter nuclei. However, missegregated chromosomes often decondense separately to form micronuclei that persist for long periods in daughter cells and can induce catastrophic DNA damage (Crasta et al., 2012; Hatch et al., 2013; Thompson and Compton, 2011; Zhang et al., 2015). We tested whether short metaphase delays increase the incidence of micronuclei. We quantified the number of micronuclei in LLC-PK cell cultures 24 h after transient arrests with MG132 or Nocodazole for 1 h and 3 h. Cells delayed at metaphase with MG132 treatment for 3 h exhibited significantly higher numbers of micronuclei compared to cells arrested for 1 h or cells treated with nocodazole for 3 h (Figures 6C and 6D).

To map the effects of short metaphase delays in greater detail, we used video microscopy. To achieve metaphase delays of varying lengths, we treated cells with 10, 20 or 30 µM ProTAME, an inhibitor of the APC/C. ProTAME delayed cells at metaphase for varying durations in a dose-dependent manner (Supplementary figure 6B). ProTAME-induced metaphase delays were followed by three outcomes: 1) normal anaphase and mitotic exit, 2) defective anaphase accompanied by lagging chromosomes, anaphase bridges, or micronuclei

or 3) cohesion fatigue (Figure 7A). Cells delayed at metaphase for less than 2 h had a low incidence (15%) of anaphase defects. The number of cells showing defective anaphase increased to 45% in cells delayed for 3 h and to approximately 60% in cells delayed for 4 h. With longer arrest durations, the number of cells exhibiting defective anaphase declined, while the number of cells that underwent chromatid separation in cohesion fatigue increased (Figures 7B and 7C). Cells exhibiting normal anaphase were delayed at metaphase an average of 134 ±111 min, while cells showing at least one kind of chromosome segregation defect were delayed for 199 ±106 min. Complete cohesion fatigue occurred in cells arrested at metaphase for 370 ±105 min (Supplementary figure 6C). Thus, cells showed an increased frequency of segregation errors that correlated with the duration of metaphase arrest but then underwent full chromatid separation after extended times at metaphase. Because massive chromatid separation reactivates the spindle checkpoint, such cells do not generally enter anaphase. Overall, limited separation of chromatids caused by metaphase delay produces chromosome segregation defects in anaphase and often generates micronuclei.

Discussion:

Our data reveal that breaching of sister chromatid cohesion that accompanies cohesion fatigue does not require release of core Cohesin ring components from chromatids. It also does not appear to exploit a specific protein-protein interface in the Cohesin ring. More specifically, the Wapl-mediated prophase pathway is not required during metaphase arrest to separate sister chromatids in cohesion fatigue. However, impairment of the prophase pathway in early mitosis leads to increased retention of Cohesin on metaphase chromosomes, which can delay cohesion fatigue onset. In contrast, compromised Cohesin in mitotic chromosome causes acceleration of cohesion fatigue. Our studies also demonstrate the dynamic tension of the mitotic spindle,

specifically the pulling forces acting on kinetochores countered by the resistance of Cohesin that holds chromatids together. The rate of chromatid separation in cells delayed at metaphase yields a quantitative measure of these two components. Our studies also reveal how transient metaphase arrest can become deleterious to fidelity of chromosome segregation.

Here we show that mitotic spindle microtubule dynamics affect cohesion fatigue, likely by modulating spindle-pulling forces. Low concentrations of Taxol accelerate fatigue, while low concentrations of Nocodazole slow it. Partial inhibition of Eg5 kinesin with STLC likely compromises overall spindle tension to relax spindle-pulling force and slow cohesion fatigue (Figure 1). These results highlight the roles of robust and dynamic microtubules and sufficient spindle-pulling forces to separate sister chromatids during cohesion fatigue.

Two previous studies suggested that experimentally induced metaphase delays could reduce immediate chromosome segregation errors (Cimini et al., 2003; Ertych et al., 2014). However, our detailed analyses indicated the opposite, that transient metaphase delays increase the incidence of segregation defects during anaphase (Figures 6B and 7B-C). The reason for this discrepancy is not clear, but we note that the previous reports used different cell lines and different experimental conditions. Consistent with the previous studies, we found that short metaphase delays did not noticeably increase the chromosome segregation errors (Supplementary figure 6C). This suggests that a critical threshold of metaphase arrest and accompanying kinetochore separation may be required before the delay becomes detrimental. In our experiments increased kinetochore separation abrogates the normal back-to-back orientation of sister kinetochores allowing greater chances for merotelic attachments of single kinetochores to both spindle poles. These kinetochores become displaced from high concentrations of Aurora B at inner centromeres, where Aurora B induces release of inappropriate microtubule attachments increasing their incidence (Liu et al., 2009). Such merotelic kinetochore attachments have been shown to increase the incidence of anaphase

defects (Cimini et al., 2003; Salmon et al., 2005; Thompson and Compton, 2011) Cohesion fatigue that generates chromatid separation in several chromosomes likely compromises cell viability either through cell cycle arrest mediated by the spindle checkpoint or through catastrophic chromosome missegregation if cells exit mitosis. Here we show that the more subtle errors that accompany partial chromatid separation for cells with shorter delays in metaphase produce segregation defects that can propagate in daughter cells.

While our results show that the prophase pathway is not required for cohesion fatigue, it may still influence timing. Complete disruption of spindle microtubules eliminates cohesion fatigue. However, extended arrest in the absence of microtubules renders cells more sensitive to subsequent cohesion fatigue when metaphase spindles are allowed to form (Figure 2B). Over time in cells arrested with depolymerized spindles, chromosome-associated Cohesin may diminish through continued action of the prophase pathway and/or background separase activity. In support of this idea, we found diminished Cohesin levels on chromosomes isolated from cells treated with high concentrations of Nocodazole for longer times (Supplementary figure 2C).

Our data also reveal that both the total amount of Cohesin and the full integrity of the Cohesin complex dictates the rate of cohesion fatigue. Previous studies showed that treatment of cell populations with siRNA to deplete the Cohesin antagonist, Wapl, increased the time these cells require to undergo chromatid separation (Daum et al., 2011; Stevens et al., 2011). In this study, using HeLa cells stably expressing SMC1-GFP, we show directly that cohesion fatigue is delayed for chromosomes enriched in Cohesin through Wapl depletion. We also show that expression of non-phosphorylatable sororin mutant delays the cohesion fatigue confirming that inhibition of prophase pathway prior to mitosis enriches cohesin on chromosome, which delays the onset of cohesion fatigue (Figures 4A and 4B).

Cohesin contains one of two auxiliary “Stromal Antigen” components, SA1 or SA2. In HCT116 and RPE1 cells, depletion of SA2 causes significant increases in lagging chromosomes (Kleyman et al., 2014). Furthermore, in HCT116 cells, knockout of the Stag2 gene, which codes for SA2, does not strongly affect normal mitotic progression but may increase the incidence of aneuploidy (Solomon et al., 2011). However, when arrested at metaphase, we found that HCT116 cells lacking SA2 underwent faster cohesion fatigue compared to parental HCT116 cells (Figure 2C). However, it does not appear that release of SA2 accompanies cohesion fatigue in normal cells, since chromatin-associated SA2 does not decrease during metaphase arrest or after chromatid separation (Figure 2D). Inactivating mutations in the Stag2 gene are correlated with aneuploidy in some cancers (Solomon et al., 2011). We propose that an increased propensity for full or partial chromatid separation due to cohesion fatigue may contribute to aneuploidy in cells with mutations in Stag2.

In isolated mitotic chromosome fractions, buffers containing moderate levels of salt release most chromosome-bound Cohesin (Bermudez et al., 2012). We speculate that the functional or “cohesive” Cohesin reflects the minor salt-resistant population. The precise molecular nature of how Cohesin holds sister chromatids together remains controversial. Most concepts are specific variations on two general modes of Cohesin/chromatin interaction termed “embrace” or “handcuff” models (reviewed in (Skibbens, 2016). Embrace models propose that both sisters are contained within the same Cohesin ring, while handcuff models suggest each sister chromatid is enclosed in separate rings that are bound together. Although sister chromatids can completely separate during cohesion fatigue, we find no change in the amount of salt-stable, core Cohesin components before or after chromatid separation (Figure 3). This result suggests that on chromosomes, salt-resistant Cohesin rings are retained on chromatids during their separation in cohesion fatigue. Although unlikely, it is formally possible that salt-resistant Cohesin might be released during separation and rebind later. Another potential

alternative is that sister chromatid cohesion is mediated only by a very small pool of Cohesin, which is released at levels we cannot detect.

One explanation for the retained Cohesin complex on chromatids during cohesion fatigue postulates that protein-protein interactions among Cohesin ring components may open transiently. If kinetochores maintain tension, then these transient openings may allow separation at sites where sisters are pulled in opposite directions. Over time, separation could progress down the length of the chromosome, which is the exact behavior observed in time lapse imaging (Daum et al., 2011). However, we found that locking individual gates after completion of prophase pathway Cohesin release, did not affect the rate of cohesion fatigue (Figure 4G). This evidence suggests that there is not one gate specifically sensitive to opening during cohesion fatigue. Because we could not lock more than one gate at a time, transient openings of multiple Cohesin protein interactions could still contribute to cohesion fatigue. In a previous study we showed, by siRNA depletion, that background Separase activity did slightly affect the timing of cohesion fatigue but was not required (Daum et al., 2011). This evidence, along with our current Aurora B inhibition studies (Figure 4C) and gate locking experiments suggest that the mechanism of cohesion fatigue is likely a novel, yet undiscovered pathway of breaching sister chromatid cohesion. Our blotting data indicate that chromatids retain Cohesin during cohesion fatigue. Further, these data, together with our results from gate locking experiments, are most consistent with data demonstrating that Cohesin is neither lost nor transiently breached during cohesion fatigue. Structural studies have not yet provided unequivocal evidence for precisely how Cohesin maintains sister chromatid cohesion. Among current models the simplest to account for our results is the handcuff model of sister chromatid attachment with two interconnected Cohesin rings each entrapping a single chromatid best reconciles these findings. We speculate that under continuous pulling of sister chromatids at metaphase, the two rings

could locally fail to counterbalance the pulling force leading to ring separation and release of the local region of the sister chromatids.

Finally, previous studies suggested that cells prone to undergo rapid cohesion fatigue showed altered distribution and reduced levels of the Cohesin protector protein, SGO1 (Tanno et al., 2015). However, both fast and slow fatiguing HeLa cells exhibited no significant reduction in SGO1 protein during cohesion fatigue when compared to metaphase levels (Supplementary figures 3D and 3E). SGO1 levels were higher at metaphase in HeLa-Fast cells compared to HeLa-Slow cells, the opposite one might expect if Sgo1 levels regulated the rate of cohesion fatigue. Taken together, our observations indicate that breaching cohesion during cohesion fatigue may not require canonical Cohesin removal mechanisms, such as the Wapl pathway or the activity of Separase. However, we believe it is highly likely that these mechanisms may influence the sensitivity and rates of cohesion fatigue in different cells and under different conditions.

Although certain cells, notably some cancer cell lines, exhibit high degrees of chromosome instability, most dividing cells in culture show low rates of spontaneous segregation errors that can manifest in several ways (Thompson and Compton, 2008). As with the other errors, we observe spontaneous cohesion fatigue in normal control cells at low frequency (data not shown). Cells that undergo substantial cohesion fatigue with many separated chromatids are likely to die, because separated single chromatids elicit spindle checkpoint signaling (Lara-Gonzalez and Taylor, 2012), which promotes continued mitotic arrest and cell death. Even if they survive and divide after delay, the progeny cells would have highly abnormal chromosome content and are likely to be inviable. In this study we also focused on less extreme circumstances, where shorter delays at metaphase allowed sister chromatids to partially separate before anaphase onset (Figure 5).

Metaphase is a point of balance between microtubule-dependent pulling forces that separate chromatids versus cohesive forces that hold chromosomes together. While normally transient, metaphase can be delayed. Our data suggest that many factors contribute to cell sensitivity to cohesion fatigue including the various canonical Cohesin regulators. However, a complete understanding of the primary molecular mechanisms underlying chromatid separation during cohesion fatigue remains unresolved and may reflect an incomplete understanding of sister chromatid cohesion. Future studies of cohesion fatigue may provide insight into the nature of Cohesin complex-chromatin interactions. While complete chromatid separation of many chromosomes will likely result in cell death or inviable progeny cells, complete separation of one or a few chromosomes and/or partial chromatid separation may be a key source of genomic instability that perpetuates the evolution of malignant cells in cancer.

Material and methods:

Cell culture and drug treatments: HeLa, LLC-PK, HCT116 and HEK293 cells were cultured in flasks in DMEM-based media supplemented with 2 mM HEPES, non-essential amino acids (NEAA), sodium-pyruvate, 1X penicillin-streptomycin (P/S, Corning, 30-002-CI) and 10% FBS. Cells were maintained at 37°C in 5% CO_2 in a water-jacketed incubator. Cells were subcultured every other day and were used within 6 months of thawing from liquid nitrogen. Unless otherwise specified, drugs were applied at the following concentrations: Nocodazole: 330 nM, MG132: 25 µM, ProTAME: 25 µM, Rapamycin: 100 nM, ZM447439: 2.5 uM. All cell lines were routinely tested for mycoplasma. HeLa cells, LLC-PK cells and HCT116 cells were mycoplasma free. The HEK293 cells were found to be mycoplasma positive. Unfortunately, all the stock cultures, even the earliest isolates at the laboratory of origin were found to be mycoplasma positive. We used several approaches designed to cure the mycoplasma contamination, but these were unsuccessful.

Chromosome/chromatin isolation: Subconfluent cultures of HeLa cells were treated with Nocodazole for 12 - 16 h, then mitotic cells were collected by shake-off. Cells remaining in the flasks (interphase cells primarily in G2) were collected by trypsinization. Cells were centrifuged in 50 ml tubes at 200 Xg for 4 min and re-suspended in warm media at 1X10^6 cells/ml. 4x10^5 cells were aliquoted into 1.5 ml micro-centrifuge tubes and centrifuged at 200 Xg for 5 min. The cell pellet was then lysed with cold Extraction Lysis Buffer (ELB) by repeated pipetting. The ELB contained PHEM buffer: 60 mM PIPES, 25 mM HEPES, 10 mM EGTA and 4 mM $MgCl_2$ with 0.1 M NaCl, 1% CHAPS, 1mM DTT, and 1:200 protease inhibitor (Sigma, P8340). Lysed cells were incubated for 20 min in ice then centrifuged at 1400 Xg for 10 min. A fraction of soluble supernatant was saved. The pellets were subjected to two more cycles of resuspension in ELB and centrifugation.

Western blot: Supernatant and chromatin pellets were dissolved in 1X loading buffer (1X LDS sample buffer (Thermofisher, NP007) + 50 mM DTT). Equivalent cell numbers were loaded on 4-12% NuPAGE gels, electrophoresed at 50 V for 7 min, then for 2 h at 150 V in MOPS SDS running buffer. Proteins were transferred onto 0.45 micron PVDF membrane in transfer buffer (50 mM Tris, 192 mM Glycine and 0.05% SDS) containing 15% methanol with a Midi transfer apparatus (Idea Scientific). Blots were blocked with 5 % non-fat dry milk in PBST (PBS with 0.05% Tween 20) or 1:10 Sea Block (Thermofisher, 37527). Blots were cut into pieces and incubated with rabbit anti-SMC3 (Bethyl, A300-055A) at 1:1000 in block, rabbit anti-RAD21 (Bethyl, A300-080A, BL331) at 1:1000, mouse anti-SA2 (Santa Cruz, J-12) at 1:1000, rabbit anti-CENPA (Millipore, 07-574) at 1:200 and rabbit anti-Histone H3 (Abcam, ab1791) at 1:10000 at 4°C overnight with gentle rocking. Blots were washed 3 times with PBST then labeled with Horseradish Peroxidase (HRP) conjugated goat anti-rabbit secondary (JacksonImmunoresearch, 11-035-144) at 1:20000. For far red fluorescent detection, goat anti-rabbit, or anti-mouse (Azure biosystem, AC2128 and AC2129) were used at 1:10000 at room temperature for 2.5 h. Blots were washed again 3 times with PBST. For HRP detection blots were treated with Pierce West Pico reagent for 5 mins, then captured by chemiluminescence with a Kodak 4000R Image Station. For far-red fluorescence, membranes were imaged using an Azure c600 imaging system. Blot quantification was done using the raw images with Metamorph Software (Molecular devices).

Chromosome spreads: Mitotic cells were washed with warm media by centrifuging at 300Xg for 3 min. Cells were suspended in 500 µl of warmed swelling buffer (40 % complete media + 60% DI water). Samples were incubated in a 37°C water bath for 15-18 min. Swollen cells were fixed by adding 1 ml 3:1 methanol: acetic acid, then incubated for 10 min. The cells were pelleted for 5 min at 250Xg, then washed with 1 ml fixative and pelleted once more. The cell pellets were resuspended in 100-200 µl fixative, then 40-50 µl of cell suspension was dropped from a height of 60 cm onto a 22 mm^2 coverslip that was cleaned with 95% ethanol and wiped

with acetic acid. The coverslips were immediately placed inside a 150 mm plastic culture dish on top of wet filter paper. The lid was left off, and the coverslips were allowed to dry in the humidified chamber. Once dried, coverslips were stained with DAPI (100 ng/ml) and SYBERGold nucleic acid dye (1:20000). Slides were imaged with a Zeiss Axioplan II microscope using a 100X objective, Hamamatsu Orca II camera and Metamorph software. At least 200 mitotic spreads were scored for each sample. If an individual cell spread had more than 10 single chromatids, the cell was scored as fatigued.

Live cell imaging: Cells were grown in chambered cover glasses (Lab-Tek) for 24 h, then the medium was changed to L-15 phenol red-free medium supplemented with P/S, NEAA and 10% FBS. The surface of the medium was overlayered with mineral oil to reduce evaporation. For most experiments, chambers were transferred to a Zeiss Axiovert microscope then imaged while using an air-curtain heater to maintain the temperature at 37°C. Images were acquired every 7-10 min for 18-20 h with a Zeiss 20X objective and ORCA-ER Hamamatsu camera using Metamorph Software (Molecular Devices LLC). Images were analyzed using Metamorph software. For experiments; Wapl depletion in SMC1-GFP cells, STLC treatment in HeLa-Fast, Taxol treatment in HeLa-Slow, Rapamycin treatment in HeK293, ZM447439 treatment, and Sororin mutant images were acquired using 20X objective in a Nikon Ti microscope fitted with an OKOlab environmental chamber. For each cell that entered mitosis, the intervals from nuclear envelope breakdown (NEBD) to metaphase and to anaphase onset or cohesion fatigue were recorded. To induce metaphase arrest, cells were treated with 25 µM MG132 or 25 µM ProTAME, and scored as fatigued when approximately 10% of the chromosomes had undergone chromatid separation.

siRNA experiments: HeLa cells stably expressing SMC1-GFP were grown on chambered cover glasses. Cells were transfected with Wapl siRNAs #1 GAGAGAUGUUUACGAGUUU; #2 CAACAGUGAAUCGAGUAA or universal negative control (Sigma catalog # SIC001) using

RNAi Max lipofectamine (Thermofisher catalog # 13778150). 48 h after transfection, live cell imaging was done as described above. Only cells that showed a clear GFP signal on metaphase chromosomes were included indicating significant depletion of Wapl. The elapsed time from NEBD to metaphase and to chromatid separation was measured.

Immunofluorescence: Cells grown on 22 mm^2 coverslips were simultaneously fixed and permeablized with 2% PFA and 0.5% Triton X-100 in 1X PHEM buffer at room temperature for 15 min. The cells were blocked with 20% boiled normal goat serum (BNGS) for at least 20 min. Coverslips were incubated with primary antibody, CREST (1:800, Antibody INC, 15-134), rabbit anti SGO1 (1:500, a gift from Dr. Hongtao Yu) diluted in 5% BNGS in PBST overnight at 4°C. Coverslips were washed 3 times with MBST (MOPS buffered saline with 0.05% Tween 20), then incubated in secondary antibody, goat anti-rabbit conjugated to CY3 at 1:1500 (JacksonImmuno, 111-165-045109) , goat anti-human conjugated to FITC at 1:800 (JacksonImmuno, 109-95-088) for 2 h at room temperature. After incubation with secondary antibodies, coverslips were washed three times again then labeled with DAPI (100 ng/ml) for one min. Coverslips were mounted on slides with Vectashield mounting media (Victor labs, H-1000), then sealed with clear nail polish. Fluorescence images of cells were taken using a Zeiss Axioplan II microscope with a Zeiss 100X objective, Hamamatsu Orca II camera and Metamorph software. Distances between pairs of kinetochores were measured using the region measurement tool in Metamorph software.

Transient metaphase arrest: For fixed cell analysis, LLC-PK cells grown on 22mm^2 were treated with 5 µM MG132 ± 330 nM Nocodazole for 3 h. Arrested cells were washed 4 times with warm DMEM then released into complete DMEM medium to complete mitosis. 3.5 h after release from drug, cells were fixed with 3:1 methanol: acetic acid and labelled with (DAPI 100 ng/ml). Anaphase cells were examined visually for lagging chromosomes or anaphase bridges with a Zeiss Axioplan II and a Zeiss 100X objective. For identification of micronuclei, LLC-PK

cells grown on coverslips were transiently arrested with Nocodazole for 3 h or MG132 for 1 or 3 h then washed and released into complete medium. 24 h after release, cells were fixed with 3:1 methanol: acetic acid then labeled with DAPI (100 ng/ml). Each coverslip was imaged at 50 random positions with a Zeiss Axiovert microscope and Zeiss 20X objective. The total number of cells and micronuclei in a field was quantified using Metamorph software. For live cell imaging, HeLa-H2B-GFP cells grown on chambered cover glasses were treated with 10, 20, or 30 µM ProTAME in L-15 medium then imaged every 10 min for 18 h. Every cell that entered the mitosis was examined visually at anaphase for any visible signs of anaphase bridges, lagging chromosomes or micronuclei formation.

Acknowledgements:

We thank Dr. Arshad Desai for HeLa cells expressing H2B-mRFP, Dr. Kyoko Yokomori for HeLa cells expressing SMC1-GFP, Dr. Todd Waldman for HCT116 SA2 knockout cells, Dr. Olaf Stemmann for HeK293 cells expressing FRB- and FKBP-fused Cohesin proteins, and Dr. Hongtao Yu for HeLa cell expressing 9A-mutnat Sororin and anti-SGO1 antibodies. Our thanks to all the members of Program in Cell Cycle and Cancer Biology at OMRF for insightful discussion and comments. This work was supported by the National Institute of General Medical Sciences (R01GM111731) and by the McCasland Foundation.

References

Bermudez, V.P., A. Farina, T.L. Higashi, F. Du, I. Tappin, T.S. Takahashi, and J. Hurwitz. 2012. In vitro loading of human cohesin on DNA by the human Scc2-Scc4 loader complex. *Proc Natl Acad Sci U S A*. 109:9366-9371.

Buheitel, J., and O. Stemmann. 2013. Prophase pathway-dependent removal of cohesin from human chromosomes requires opening of the Smc3-Scc1 gate. *Embo j*. 32:666-676.

Canudas, S., and S. Smith. 2009. Differential regulation of telomere and centromere cohesion by the Scc3 homologues SA1 and SA2, respectively, in human cells. *J Cell Biol*. 187:165-173.

Cimini, D., B. Moree, J.C. Canman, and E.D. Salmon. 2003. Merotelic kinetochore orientation occurs frequently during early mitosis in mammalian tissue cells and error correction is achieved by two different mechanisms. *J Cell Sci*. 116:4213-4225.

Crasta, K., N.J. Ganem, R. Dagher, A.B. Lantermann, E.V. Ivanova, Y. Pan, L. Nezi, A. Protopopov, D. Chowdhury, and D. Pellman. 2012. DNA breaks and chromosome pulverization from errors in mitosis. *Nature*. 482:53-58.

Daum, J.R., T.A. Potapova, S. Sivakumar, J.J. Daniel, J.N. Flynn, S. Rankin, and G.J. Gorbsky. 2011. Cohesion fatigue induces chromatid separation in cells delayed at metaphase. *Curr Biol*. 21:1018-1024.

Ertych, N., A. Stolz, A. Stenzinger, W. Weichert, S. Kaulfuss, P. Burfeind, A. Aigner, L. Wordeman, and H. Bastians. 2014. Increased microtubule assembly rates influence chromosomal instability in colorectal cancer cells. *Nat Cell Biol*. 16:779-791.

Gandhi, R., P.J. Gillespie, and T. Hirano. 2006. Human Wapl is a cohesin-binding protein that promotes sister-chromatid resolution in mitotic prophase. *Curr Biol*. 16:2406-2417.

Haarhuis, J.H., A.M. Elbatsh, B. van den Broek, D. Camps, H. Erkan, K. Jalink, R.H. Medema, and B.D. Rowland. 2013. WAPL-mediated removal of cohesin protects against segregation errors and aneuploidy. *Curr Biol*. 23:2071-2077.

Haarhuis, J.H.I., R.H. van der Weide, V.A. Blomen, J.O. Yanez-Cuna, M. Amendola, M.S. van Ruiten, P.H.L. Krijger, H. Teunissen, R.H. Medema, B. van Steensel, T.R. Brummelkamp, E. de Wit, and B.D. Rowland. 2017. The Cohesin Release Factor WAPL Restricts Chromatin Loop Extension. *Cell*. 169:693-707.e614.

Hatch, E.M., A.H. Fischer, T.J. Deerinck, and M.W. Hetzer. 2013. Catastrophic nuclear envelope collapse in cancer cell micronuclei. *Cell*. 154:47-60.

Hauf, S., E. Roitinger, B. Koch, C.M. Dittrich, K. Mechtler, and J.M. Peters. 2005. Dissociation of cohesin from chromosome arms and loss of arm cohesion during early mitosis depends on phosphorylation of SA2. *PLoS Biol*. 3:e69.

Hou, F., C.W. Chu, X. Kong, K. Yokomori, and H. Zou. 2007. The acetyltransferase activity of San stabilizes the mitotic cohesin at the centromeres in a shugoshin-independent manner. *J Cell Biol*. 177:587-597.

Kleyman, M., L. Kabeche, and D.A. Compton. 2014. STAG2 promotes error correction in mitosis by regulating kinetochore-microtubule attachments. *J Cell Sci*. 127:4225-4233.

Kueng, S., B. Hegemann, B.H. Peters, J.J. Lipp, A. Schleiffer, K. Mechtler, and J.-M. Peters. Wapl Controls the Dynamic Association of Cohesin with Chromatin. *Cell*. 127:955-967.

Lara-Gonzalez, P., and S.S. Taylor. 2012. Cohesion fatigue explains why pharmacological inhibition of the APC/C induces a spindle checkpoint-dependent mitotic arrest. *PLoS One*. 7:e49041.

Liu, D., G. Vader, M.J. Vromans, M.A. Lampson, and S.M. Lens. 2009. Sensing chromosome bi-orientation by spatial separation of aurora B kinase from kinetochore substrates. *Science*. 323:1350-1353.

Liu, H., L. Jia, and H. Yu. 2013a. Phospho-H2A and cohesin specify distinct tension-regulated Sgo1 pools at kinetochores and inner centromeres. *Curr Biol*. 23:1927-1933.

Liu, H., S. Rankin, and H. Yu. 2013b. Phosphorylation-enabled binding of SGO1-PP2A to cohesin protects sororin and centromeric cohesion during mitosis. *Nat Cell Biol*. 15:40-49.

McGuinness, B.E., T. Hirota, N.R. Kudo, J.M. Peters, and K. Nasmyth. 2005. Shugoshin prevents dissociation of cohesin from centromeres during mitosis in vertebrate cells. *PLoS Biol*. 3:e86.

Michaelis, C., R. Ciosk, and K. Nasmyth. 1997. Cohesins: chromosomal proteins that prevent premature separation of sister chromatids. *Cell*. 91:35-45.

Murayama, Y., and F. Uhlmann. 2015. DNA Entry into and Exit out of the Cohesin Ring by an Interlocking Gate Mechanism. *Cell*. 163:1628-1640.

Nishiyama, T., R. Ladurner, J. Schmitz, E. Kreidl, A. Schleiffer, V. Bhaskara, M. Bando, K. Shirahige, A.A. Hyman, K. Mechtler, and J.M. Peters. 2010. Sororin mediates sister chromatid cohesion by antagonizing Wapl. *Cell*. 143:737-749.

Nishiyama, T., M.M. Sykora, P.J. Huis in 't Veld, K. Mechtler, and J.M. Peters. 2013. Aurora B and Cdk1 mediate Wapl activation and release of acetylated cohesin from chromosomes by phosphorylating Sororin. *Proc Natl Acad Sci U S A*. 110:13404-13409.

Sackton, K.L., N. Dimova, X. Zeng, W. Tian, M. Zhang, T.B. Sackton, J. Meaders, K.L. Pfaff, F. Sigoillot, H. Yu, X. Luo, and R.W. King. 2014. Synergistic blockade of mitotic exit by two chemical inhibitors of the APC/C. *Nature*. 514:646-649.

Salmon, E.D., D. Cimini, L.A. Cameron, and J.G. DeLuca. 2005. Merotelic kinetochores in mammalian tissue cells. *Philos Trans R Soc Lond B Biol Sci*. 360:553-568.

Shintomi, K., and T. Hirano. 2009. Releasing cohesin from chromosome arms in early mitosis: opposing actions of Wapl-Pds5 and Sgo1. *Genes Dev*. 23:2224-2236.

Skibbens, R.V. 2016. Of Rings and Rods: Regulating Cohesin Entrapment of DNA to Generate Intra- and Intermolecular Tethers. *PLoS Genet*. 12:e1006337.

Skoufias, D.A., S. DeBonis, Y. Saoudi, L. Lebeau, I. Crevel, R. Cross, R.H. Wade, D. Hackney, and F. Kozielski. 2006. S-trityl-L-cysteine is a reversible, tight binding inhibitor of the human kinesin Eg5 that specifically blocks mitotic progression. *J Biol Chem*. 281:17559-17569.

Solomon, D.A., T. Kim, L.A. Diaz-Martinez, J. Fair, A.G. Elkahloun, B.T. Harris, J.A. Toretsky, S.A. Rosenberg, N. Shukla, M. Ladanyi, Y. Samuels, C.D. James, H. Yu, J.S. Kim, and T. Waldman. 2011. Mutational inactivation of STAG2 causes aneuploidy in human cancer. *Science*. 333:1039-1043.

Stevens, D., R. Gassmann, K. Oegema, and A. Desai. 2011. Uncoordinated loss of chromatid cohesion is a common outcome of extended metaphase arrest. *PLoS One*. 6:e22969.

Sumara, I., E. Vorlaufer, C. Gieffers, B.H. Peters, and J.M. Peters. 2000. Characterization of vertebrate cohesin complexes and their regulation in prophase. *J Cell Biol*. 151:749-762.

Tanno, Y., H. Susumu, M. Kawamura, H. Sugimura, T. Honda, and Y. Watanabe. 2015. The inner centromere-shugoshin network prevents chromosomal instability. *Science*. 349:1237-1240.

Tedeschi, A., G. Wutz, S. Huet, M. Jaritz, A. Wuensche, E. Schirghuber, I.F. Davidson, W. Tang, D.A. Cisneros, V. Bhaskara, T. Nishiyama, A. Vaziri, A. Wutz, J. Ellenberg, and J.M. Peters. 2013. Wapl is an essential regulator of chromatin structure and chromosome segregation. *Nature*. 501:564-568.

Thompson, S.L., and D.A. Compton. 2008. Examining the link between chromosomal instability and aneuploidy in human cells. *J Cell Biol*. 180:665-672.

Thompson, S.L., and D.A. Compton. 2010. Proliferation of aneuploid human cells is limited by a p53-dependent mechanism. *J Cell Biol*. 188:369-381.

Thompson, S.L., and D.A. Compton. 2011. Chromosome missegregation in human cells arises through specific types of kinetochore-microtubule attachment errors. *Proc Natl Acad Sci U S A*. 108:17974-17978.

Vallot, A., I. Leontiou, D. Cladiere, W. El Yakoubi, S. Bolte, E. Buffin, and K. Wassmann. 2017. Tension-Induced Error Correction and Not Kinetochore Attachment Status Activates the SAC in an Aurora-B/C-Dependent Manner in Oocytes. *Curr Biol*.

van der Lelij, P., S. Lieb, J. Jude, G. Wutz, C.P. Santos, K. Falkenberg, A. Schlattl, J. Ban, R. Schwentner, T. Hoffmann, H. Kovar, F.X. Real, T. Waldman, M.A. Pearson, N. Kraut, J.M. Peters, J. Zuber, and M. Petronczki. 2017. Synthetic lethality between the cohesin subunits STAG1 and STAG2 in diverse cancer contexts. *Elife*. 6.

Waizenegger, I.C., S. Hauf, A. Meinke, and J.-M. Peters. 2000. Two Distinct Pathways Remove Mammalian Cohesin from Chromosome Arms in Prophase and from Centromeres in Anaphase. *Cell*. 103:399-410.

Whelan, G., E. Kreidl, G. Wutz, A. Egner, J.M. Peters, and G. Eichele. 2012. Cohesin acetyltransferase Esco2 is a cell viability factor and is required for cohesion in pericentric heterochromatin. *Embo j*. 31:71-82.

Xu, B., S. Lu, and J.L. Gerton. 2014. Roberts syndrome: A deficit in acetylated cohesin leads to nucleolar dysfunction. *Rare Dis*. 2:e27743.

Xu, Z., B. Cetin, M. Anger, U.S. Cho, W. Helmhart, K. Nasmyth, and W. Xu. 2009. Structure and function of the PP2A-shugoshin interaction. *Mol Cell*. 35:426-441.

Zhang, C.Z., A. Spektor, H. Cornils, J.M. Francis, E.K. Jackson, S. Liu, M. Meyerson, and D. Pellman. 2015. Chromothripsis from DNA damage in micronuclei. *Nature*. 522:179-184.

Zhang, N., S.G. Kuznetsov, S.K. Sharan, K. Li, P.H. Rao, and D. Pati. 2008. A handcuff model for the cohesin complex. *J Cell Biol*. 183:1019-1031.

Figure Legends

Figure 1: Microtubule dynamics and spindle tension impact cohesion fatigue.

HeLa-Slow and HeLa-Fast cells arrested at metaphase with MG132 or ProTAME and treated with low concentrations of microtubule-poisoning drugs. The elapsed time from metaphase to chromatid scattering/cohesion fatigue (Meta-Fatigue) was determined using live cell imaging. (A and B) Treatment of HeLa-Slow and HeLa-Fast cells with MG132 ±Nocodazole (5 nM). **(C** and **D)** Treatment of HeLa-Slow and HeLa-Fast cells with ProTAME ±Taxol (1.5 nM). **(E** and **F)** Treatment of HeLa-Slow and HeLa-Fast cells with ProTAME± STLC (1.5 uM). Three independent experiments with a total of ≥150 cells were scored for each treatment and cell type. Error bars show standard deviation. The Mann-Whitney test was used for statistical analysis. Treatments that destabilize microtubules (Nocodazole) or decrease spindle tension (STLC) slowed the onset of cohesion fatigue. Conversely stabilization of microtubules with Taxol promoted faster cohesion fatigue.

Figure 2: Altering Cohesin changes the rate of cohesion fatigue.

(A) Experimental scheme for (B). **(B)** Chromosome spreads prepared from LLC-PK cells arrested in mitosis for 5 or 11 h with 330 nM Nocodazole, then washed and treated with MG132 ±Nocodazole (330 nM) for 3 or 6 h. Three independent experiments with a total of >600 spreads were scored for each treatment. Cells initially arrested for 11 h undergo more rapid cohesion fatigue than those arrested for 5 h, consistent with the continued action of the prophase pathway in removing Cohesin from chromosomes in cells arrested in mitosis. Error bars show standard deviation. Two-way ANOVA with Sidak's multiple test was used for statistical analysis. **(C)** SA2 knockout HCT116 cells underwent cohesion fatigue more rapidly than parental cells. Chromosome spreads were examined in parental and SA2 knockout HCT116 cells. Cells were treated with 330 nM Nocodazole overnight (16 h), then mitotic cells

were collected, washed then treated with MG132 ±Nocodazole (330 nM) for 3 or 6 h. Three independent experiments with totals of >600 spreads were scored. Two-way ANOVA with Sidak's multiple test was used for statistical analysis. **(D)** Immunoblotting of SA2 protein in chromosome fractions prepared from mitotic HeLa cells treated with MG132 ±Nocodazole for 8 h. Lane 1 shows baseline SA2 levels in mitotic chromosomes, lane 2 shows SA2 in chromosome fractions from fatigued chromatids and lane 3 shows cohesion fatigue negative control (MG132 plus 330 nM Nocodazole for 8 h). SA2 protein was not lost from chromatids during cohesion fatigue.

Figure 3: **The core Cohesin protein SMC3 remains bound to chromatids during cohesion fatigue.**

(**A)** Cohesion fatigue was assessed in HeLa cells stably expressing H2B-GFP treated with either DMSO (control) or ProTAME via live cell imaging. Time 0 indicates nuclear envelop breakdown (NEBD). DMSO-treated cells progress through normal mitosis (top panels), while ProTAME-treated cells undergo cohesion fatigue (bottom panels). **(B)** Chromosome spreads prepared from HeLa cells treated with MG132 ±Nocodazole for 8 h. Left panel shows paired sister chromatids (MG132+Nocodazole). Right panel shows separated sister chromatids (cohesion fatigue) after 8 h of metaphase arrest (MG132). **(C)** Immuno-blotting of chromosome fractions of mitotic HeLa cells treated with MG132 ±Nocodazole for 8 h. Lane 1 shows baseline salt-resistant SMC3 level in mitotic chromosomes before cohesion fatigue. Lane 2 reflects SMC3 in chromosome fractions of fatigued chromatids. Lane 3 shows SMC3 in negative control for cohesion fatigue (MG132 +Nocodazole). **(D)** Quantified immunoblots from four independent experiments where band intensity of SMC3 was measured and normalized to CENP-A band intensity. Kruskal-Wallis test with Dunn's multiple comparison was used for statistical analysis. Error bars represent standard deviation.

Figure 4: The prophase pathway is not required for cohesion fatigue.

(A) Elapsed times from metaphase to chromatid separation/cohesion fatigue were determined via live cell imaging in HeLa cells stably expressing SMC1-GFP. In Wapl-depleted cells, only cells with clear GFP signal on chromosomes at the metaphase plate (indicating successful Wapl depletion) were scored in two independent experiments with totals of >100 cells. **(B)** Elapsed times from metaphase to cohesion fatigue were determined in HeLa cells expressing either WT sororin or non-phosphorylatable 9A-sororin. At least 60 cells were scored for each cell type. The Mann-Whitney test was used for statistical analysis. **(C)** Experimental scheme for D. **(D)** Elapsed times from metaphase to cohesion fatigue were determined after 2.5 uM ZM 447439 treatment in 1 h metaphase arrested cells. Three independent experiments with totals of >200 cells were quantified. Inhibition of Aurora B with ZM did not cause significant delay in fatigue. The Mann-Whitney test was used for statistical analysis. **(E)** Experimental scheme for F and G. **(F)** Chromosome spreads were quantified in Hek293 gate-locking cells treated with Rapamycin to lock specific gates **prior to** prophase pathway then treated MG132 for 6 h. Totals of >100 spreads per condition per cell line were quantified. Graph shows mean±S.E.M.**(G)** Chromosome spreads were quantified in HEK293 cells with different Cohesin gates locked **after** prophase pathway in three independent experiments with totals of > 450 spreads per cells line for each treatment. Graph shows Mean±S.D. Two-way ANOVA with Tukey's multiple comparison test was used for statistical analysis. Locking the prophase-pathway gate (SMC3-RAD21) early in mitosis to inhibit the prophase pathway decreased cohesion fatigue, but locking it after the prophase pathway had occurred had no effect on cohesion fatigue.

Figure 5: Sister kinetochores begin to separate after transient metaphase arrest.

(A) Representative immunofluorescence images of LLC-PK cells either at unperturbed metaphase or arrested at metaphase for 3 h. CREST antibody-labeled kinetochores and DAPI-labeled DNA. **(B)** The average distance between pairs of kinetochores from (A) was determined in LLC-PK cells arrested in metaphase for 1 or 3 h (n ≥ 125 kinetochore pairs in 5 cells from

each treatment). One-way ANOVA, with Tukey's multiple comparison test was used for statistical analysis. **(C**) The frequency distribution of distances between pairs of kinetochores from (B) was plotted. **(D)** Live cell imaging determined the maximum stretching of sister kinetochores in LLC-PK cells arrested at metaphase for 1 or 3 h. For these measurements, n ≥ 10 pairs of kinetochore were imaged every 10 sec for 3 min. Kruskal-Wallis test with Dunn's multiple comparison was used for statistical analysis. Transient metaphase arrest led to extended separation and stretching of kinetochores, which indicated partial loss of sister kinetochore attachment.

Figure 6: Transient metaphase delays induce segregation defects in LLC-PK cells.

(A) Representative images of LLC-PK cells with segregation defects (lagging, anaphase-bridge or micronuclei) at anaphase/telophase in cells transiently arrested at metaphase. **(B)** Segregation defects during anaphase were examined in untreated cells or in cells transiently treated with Nocodazole, MG132, or MG132 +Nocodazole for 3 h in three independent experiments with >700 anaphases examined for each treatment. Error bars represent standard deviations. Ordinary one-way ANOVA with Holm-Sidak's multiple comparison test was used for statistical analysis. **(C)** Low magnification images of LLC-PK cells transiently arrested at a prometaphase-like state with nocodazole treatment or at metaphase with MG132 for 3 h then released for 24 h. Arrows indicate the micronuclei present in cells that were transiently delayed at metaphase. **(D)** Percentages of micronuclei in images from (C) were determined in ≥5000 cells from 50 randomly selected fields. One-way ANOVA was used for statistical analysis. Transient delays at metaphase caused chromosome segregation defects during anaphase and generated micronuclei. These were signifcantly reduced when Nocodazole was used to disrupt spindle pulling forces.

Figure 7: Segregation defects in HeLa cells scale with the length of metaphase delay.

(A) Live-cell images of HeLa-H2B-GFP cells treated with 10 or 20 uM ProTAME. Top panel shows a normal anaphase; middle panel shows anaphase defect (arrow shows a lagging chromosome), and bottom panel shows a fatigued cell after delay at metaphase. **(B)** Line graph shows the fate of individual cells after ProTAME treatment. Most cells with slight delays had no segregation defects, intermediate delays led to defective anaphase and longer delays resulted in cohesion fatigue. **(C)** Fractions of cells with normal anaphase, anaphase with segregation defects or cohesion fatigue were determined in cells treated with ProTAME.

Supplemental Figure Legends

Supplemental figure 1: HeLa-Fast and HeLa–Slow cells differ in fatigue kinetics, and Hela-Slow cells undergo slower mitosis in low concentrations of spindle drugs.

(A) The elapsed time from metaphase to chromatid separation (cohesion fatigue) was determined from live cell imaging in HeLa-Slow and HeLa-Fast cells treated with 25 uM ProTAME. Average time of fatigue with standard deviation is shown from three independent experiments with ≥300 cells. Mann-Whitney test was used for statistical analysis. **(B)** Kinetics of cohesion fatigue in cells from (A). **(C)** Elapsed time from NEBD to anaphase was determined by live cell imaging in HeLa-Slow cells treated with low concentrations of Nocodazole (5 nM) or Taxol (1.5 nM) showing slowed progression through mitosis. **(D)** Elapsed time from NEBD to anaphase determined with HeLa-Slow cells treated with STLC (1.5 µM) with ≥100 cells per treatment scored. All drugs slowed mitotic progression in both HeLa-Slow and HeLa-Fast cells.

Supplemental figure 2: The amount of Cohesin is altered in cells with weaker Cohesin ring or in cells lacking Wapl.

(A) Chromosome spreads were prepared from cells arrested in mitosis. The left panel shows a representative chromosome spread of a cell arrested in Nocodazole for 3h, and the right panel shows a representative spread after a 14h Nocodazole arrest. Longer arrest resulted in greater separation of chromosome arms. **(B)** Elapsed time from metaphase to cohesion fatigue in STLC+ProTAME-treated cells plotted against NEBD to chromosome alignment (metaphase). Cells that took longer to align their chromosomes fatigued faster. **(C)** Immunoblot of chromosome fractions from mitotic HeLa cells arrested in mitosis with Nocodazole for 5h or 11h. Graph shows quantification. Moderate reduction of Cohesin was detected with longer arrest. **(D)** Immunoblot of whole cell lysates of SA2 knockout HCT116 cells and parental HCT116 cells. SA2 was not detected in knockout cells and was present in parental cells. **(E)** Immunoblot of

chromosome fractions from HCT116 SA2 knockout and parental cells. Graph shows band intensity of SMC3 and RAD21 relative to CENP-A. Cohesin protein levels are reduced in SA2 knockout cells relative to parental cells.

Supplemental figure 3: Buffers containing moderate levels of salt removes most Cohesin from isolated mitotic chromosomes, and Sgo1 levels do not correlate with cohesion fatigue.

(A) Titration of Cohesin SMC33 and CENP-A used for quantitation of Cohesin proteins. Dilutions of the 0 h sample were blotted with samples from other treatments and time points. The linear ranges of dilutions were determined for accurate quantification of the Cohesin component SMC3 (top) and loading control CENP-A (bottom). **(B)** Immunoblot of Cohesin components (SMC3 and RAD21) from chromosome/chromatin fractions of mitotic and interphase (G2) HeLa cells isolated in buffers with increasing NaCl. Cohesin was readily released from mitotic chromosomes compared to interphase chromatin by salt treatment. More than 90% of Cohesin was released from mitotic chromosomes by treatment with 100 mM NaCl. **(C)** Total SGO1 levels relative to CREST signals were determined by immunofluorescence in HeLa-Slow and HeLa-Fast cells. At least 10 cells for each cell line were quantified. **(D)** SGO1 levels determined by immunofluorescence in HeLa-Slow cells that were treated with MG132 for 6h. **(E)** Total SGO1 levels in HeLa-Fast cells treated with MG132 for 3h. For each cell line and treatment, at least 5 randomly selected cells were imaged with 0.5 µm Z sections. Summed projections were generated with Metamorph Software using the stack arithmetic tool. Region of DAPI staining was used as the mask to quantify total chromosome-associated SGO1.

Supplemental figure 4: Inhibition of the prophase pathway before mitotic entry enriches chromosome-bound Cohesin and delays cohesion fatigue.

(A) Images from live cell imaging of HeLa-SMC1-GFP cells depleted of Wapl by RNAi. Wapl-depletion resulted in cells showing strong SMC1-GFP signals on mitotic chromosomes. **(B)** The elapsed time from NEBD to metaphase was determined in Hells treated with 0.5 uM ZM447439. ZM Treatment caused significant delay in chromosome alignment indicating Aurora B inhibition. >100 cells for each treatment were scored. **(C)** Chromosome spread on the left shows unresolved chromosome arms in a cell where prophase pathway was blocked by locking SMC3-RAD21 interface. Spread on right is from a control cell of the same type without Rapamycin addition (unlocked SMC3-RAD21 gate). **(D)** Percentages of chromosome spreads with closed/unresolved chromosome arms in HEK293 cells expressing pairs of Cohesin fusions to which rapamycin was added to lock different Cohesin gates. Unresolved arms were increased only when the SMC-RAD21 gate was locked. **(E)** Elapsed times form metaphase to cohesion fatigue were determined in three gate-locking Hek293 cells line with gates locked prior to mitotic entry. Locking the SMC3-RAD21 gate but not other gates delayed cohesion fatigue.

Supplemental figure 5: Short metaphase arrest causes increased interkinetochore distance only in the presence of a functional spindle.

(A) Interkinetochore distances were measured in LLC-PK cells treated with MG132 and Nocodazole for 1 or 3 h compared to normal metaphase (Control). A total of ≥100 kinetochore pairs from 5 cells were measured. One-way ANOVA was used for statistical analysis. **(B)** Interkinetochore distances were measured in HeLa cells arrested at metaphase with MG132 for 30 min or 3 h. A total of ≥100 kinetochore pairs from 5 cells were measured. **(C)** Interkinetochore distances were determined from live cell imaging in LLC-PK cells stably expressing Topo-II-GFP. Cells were arrested in metaphase with MG132 treatment for 1 or 3 h. Transient metaphase arrest led to significant kinetochore separation if spindle microtubules were intact.

Supplemental figure 6: MG132 and ProTAME induce metaphase delays whose duration determines cell fate.

(A) Percentages of defective anaphases in LLC-PK cells treated with MG132 for 1 or 4 h then released into drug-free medium. **(B)** Metaphase arrest durations were determined from live cell imaging of HeLa-Slow cells treated with increasing concentrations of ProTAME. For each concentration of ProTAME, ≥75 cells were scored. The Kruskal-Wallis test was used for statistical analysis. **(C)** The average length of metaphase arrest was determined in cells from **(B)** that exited mitosis to 1) normal anaphase, 2) defective anaphase or 3) cohesion fatigue.

Figure_1

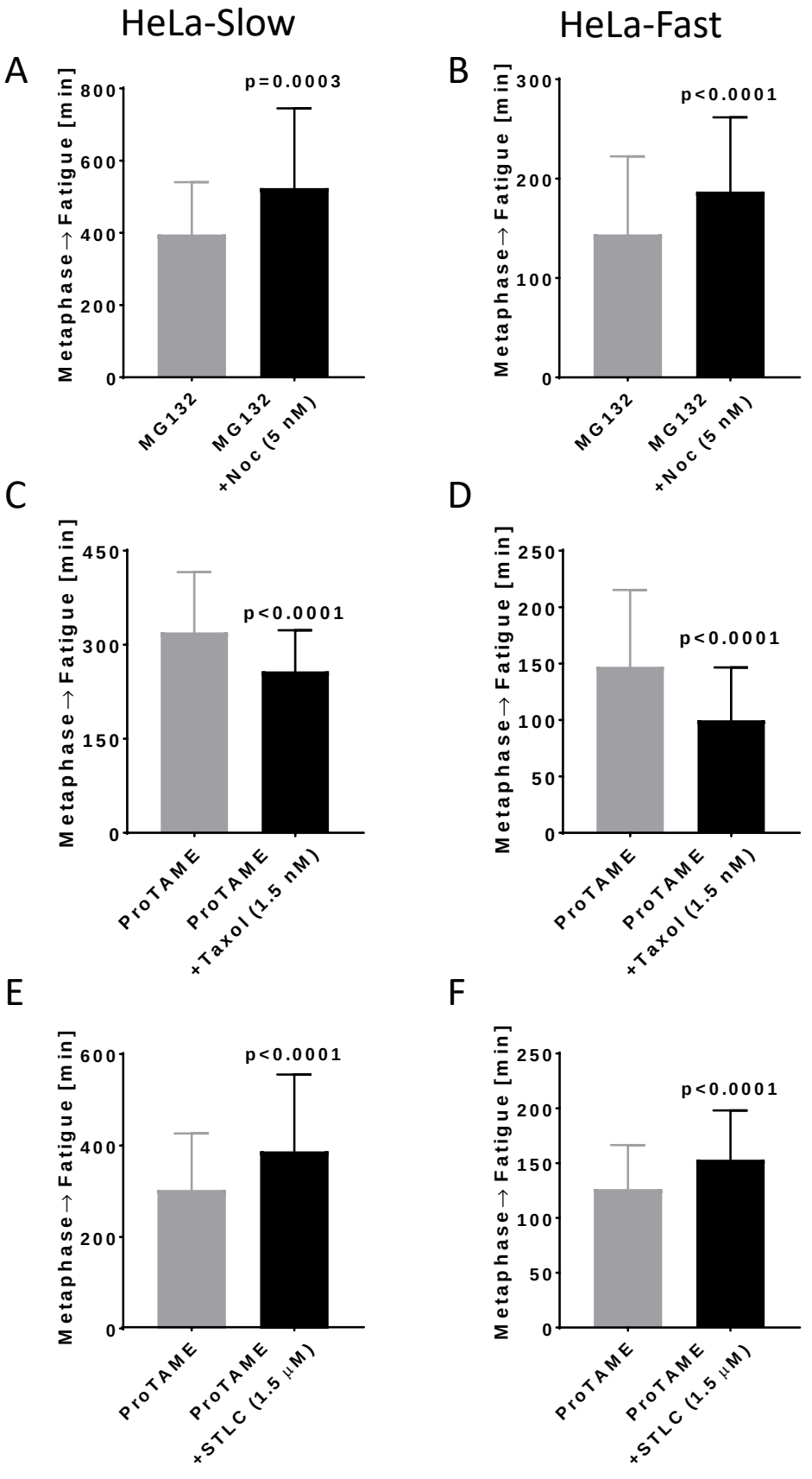
HeLa-Slow
HeLa-Fast
A
B
C
D
E
F
Metaphase→Fatigue [min]
p=0.0003
p<0.0001
MG132
MG132 +Noc (5 nM)
ProTAME
ProTAME +Taxol (1.5 nM)
ProTAME +STLC (1.5 μM)

Figure_2

A

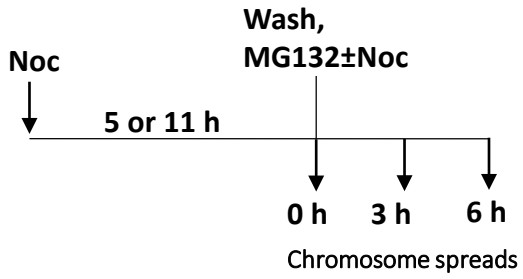

B

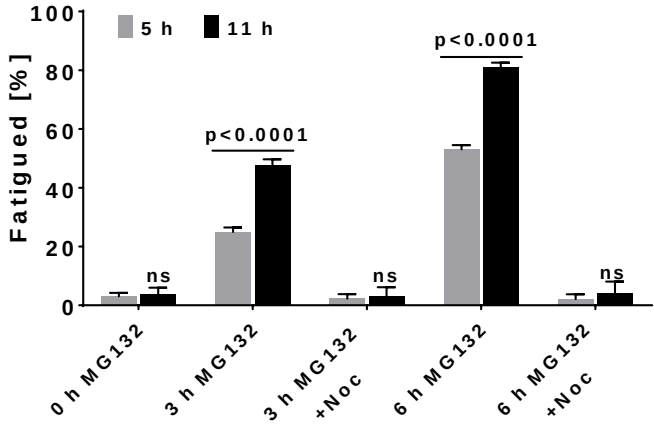

C

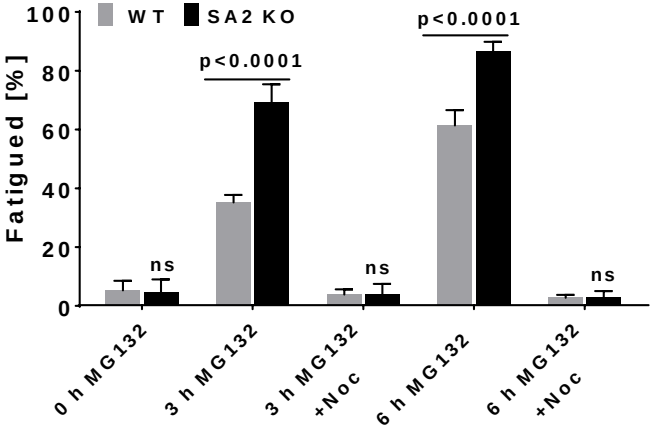

D

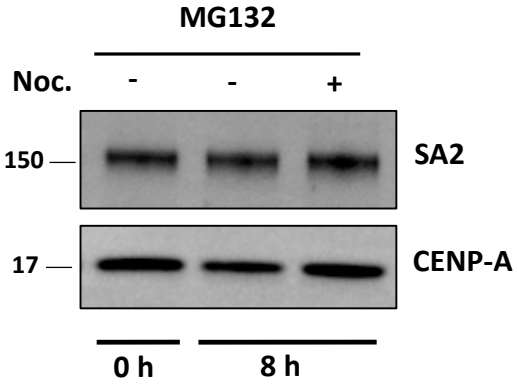

Figure_3

A

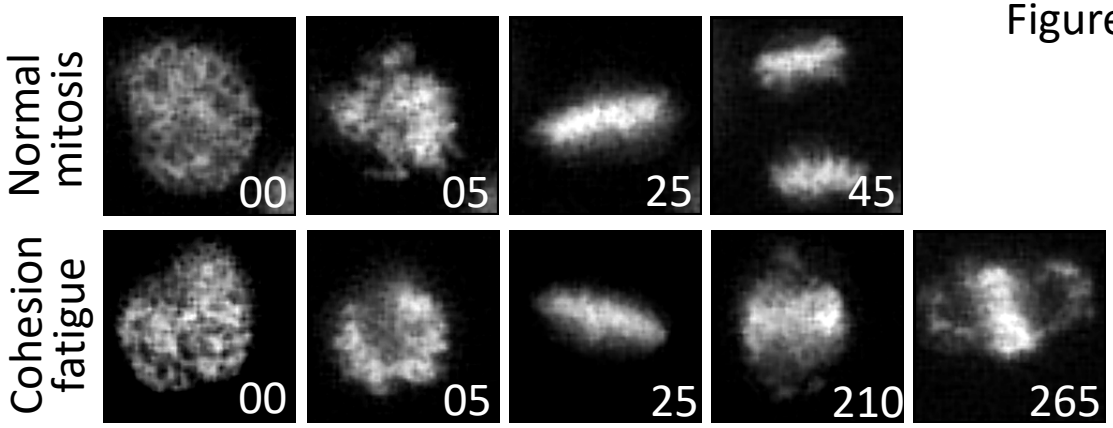

B

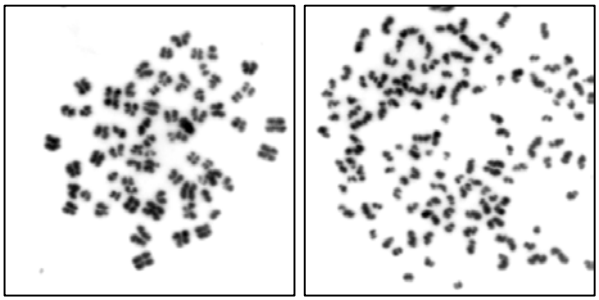

C

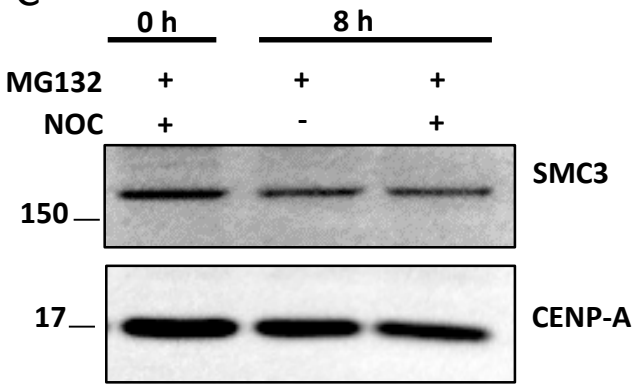

D

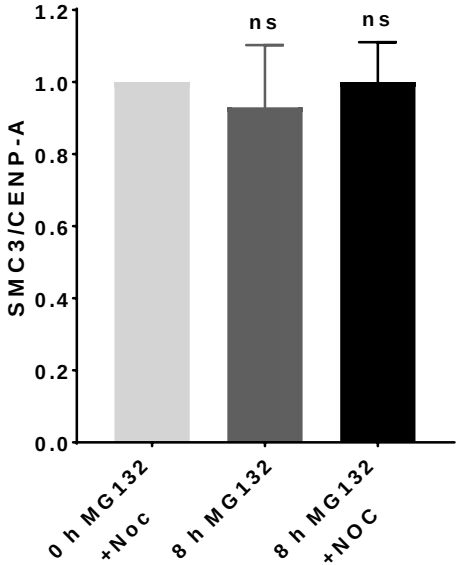

Figure_4

A

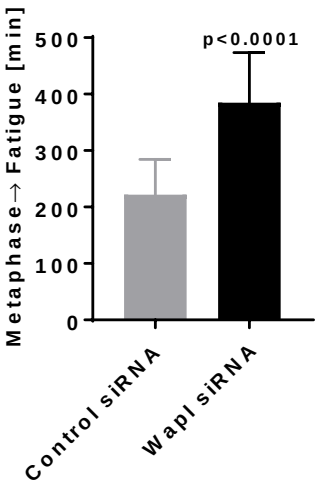

B

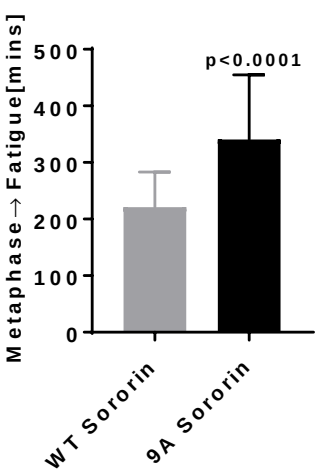

C

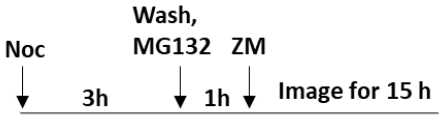

D

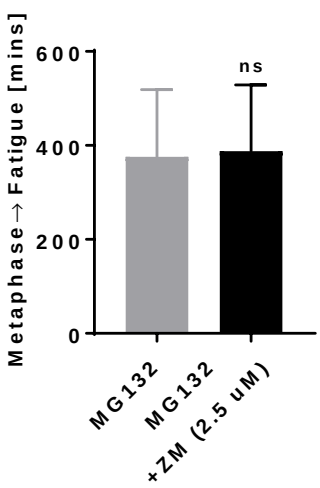

E

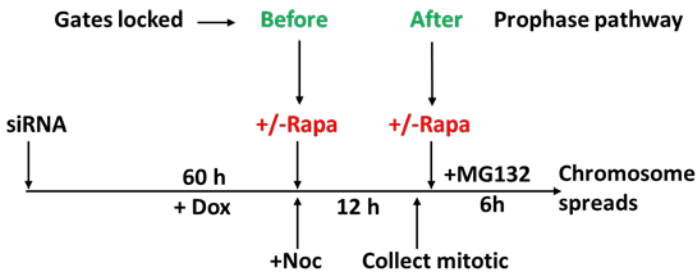

F

Gates locked **before** prophase pathway

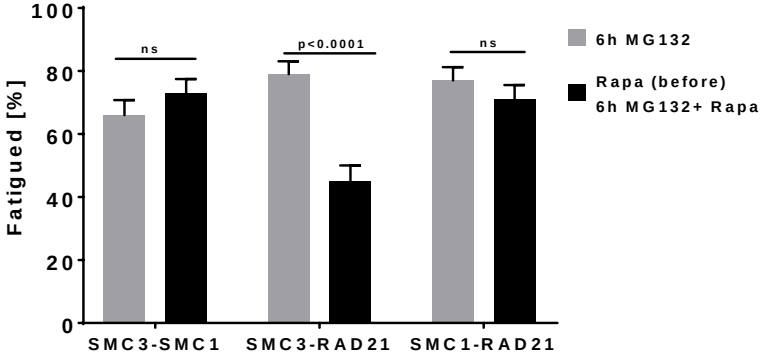

G

Gates locked **after** prophase pathway

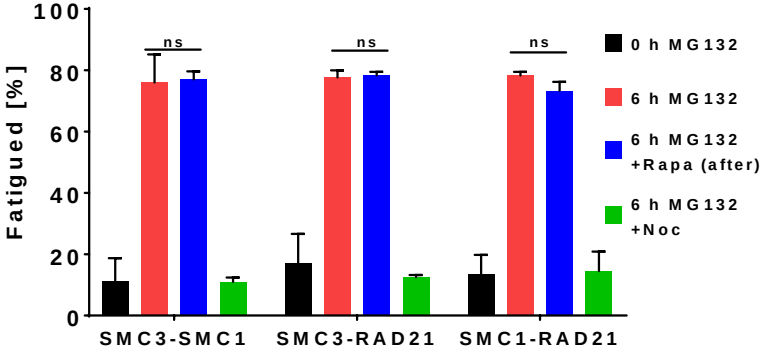

Figure_5

A

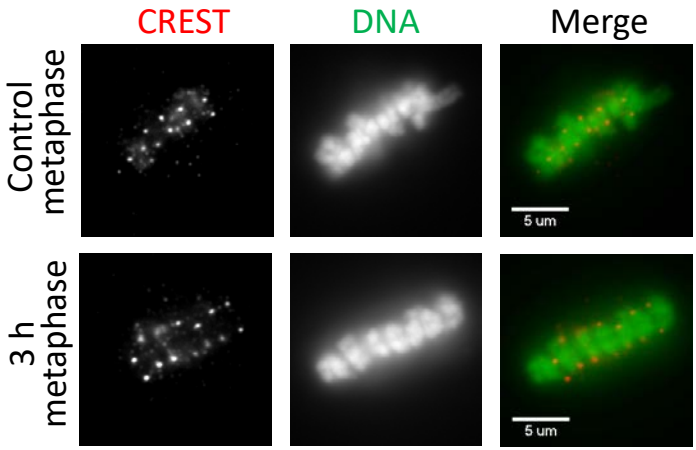

B

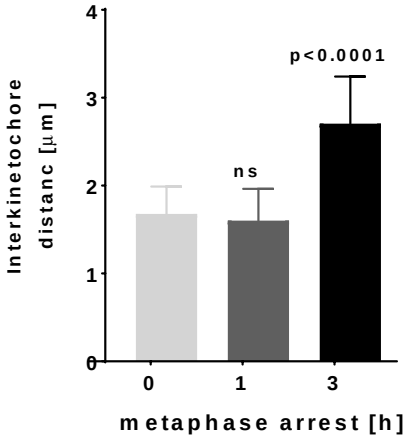

C

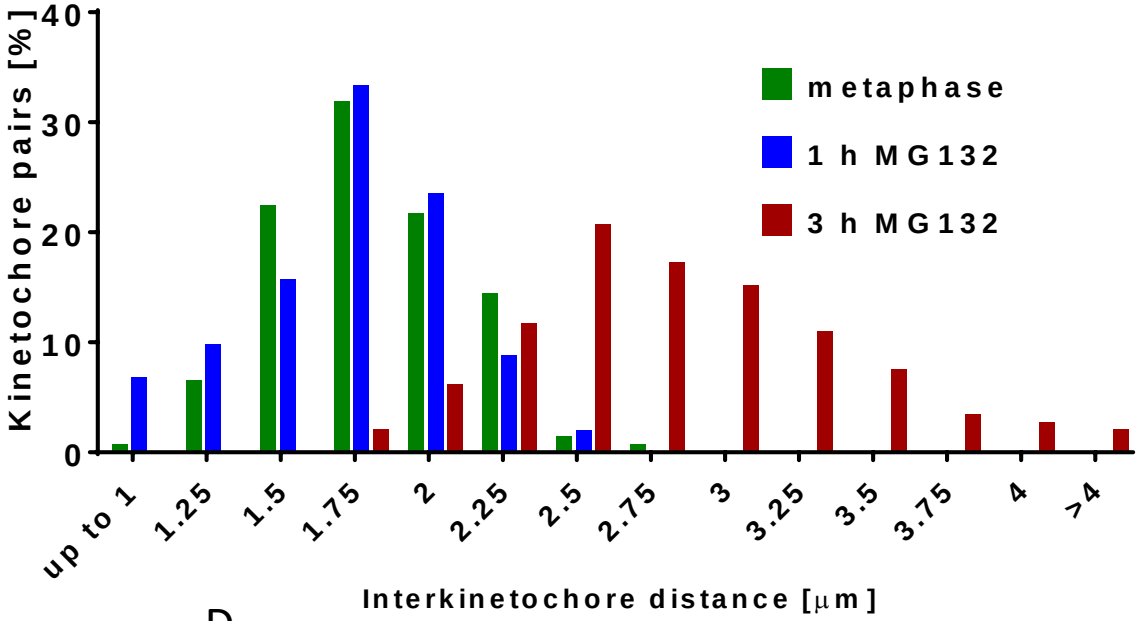

D

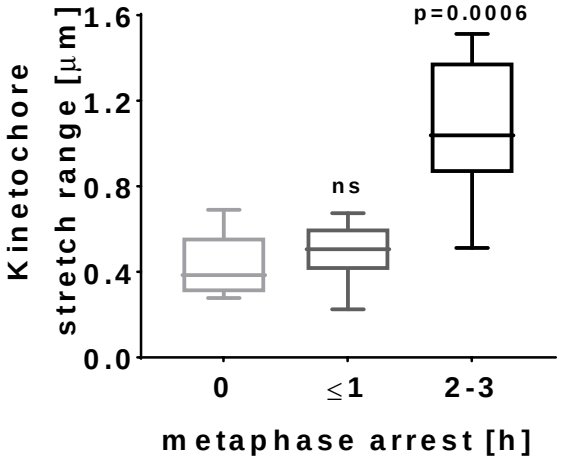

Figure_6

A

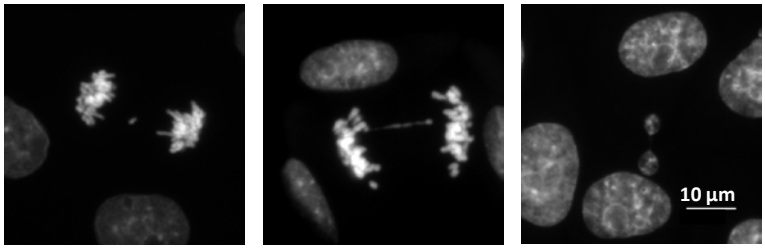

Lagging Anaphase bridge Micronuclei

B

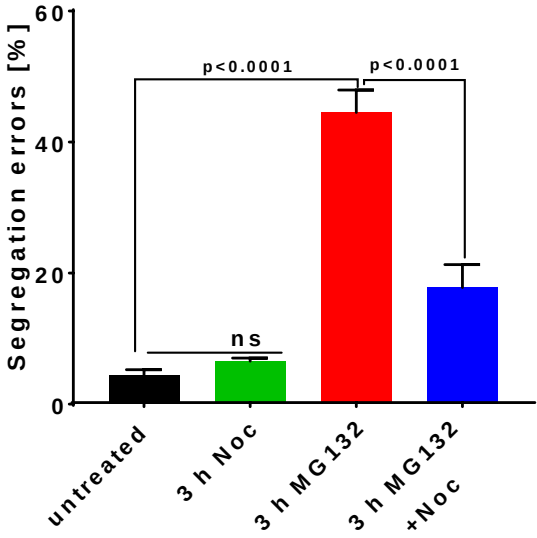

C

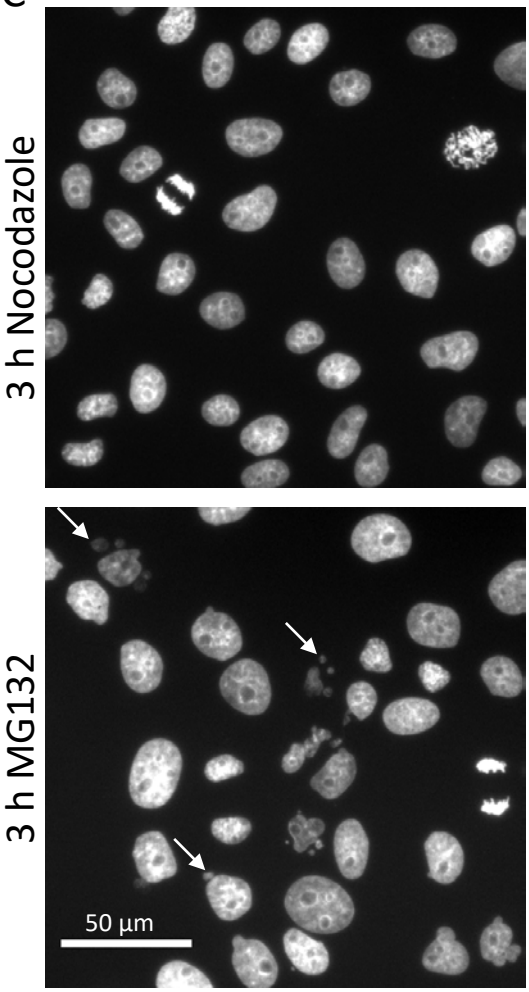

D

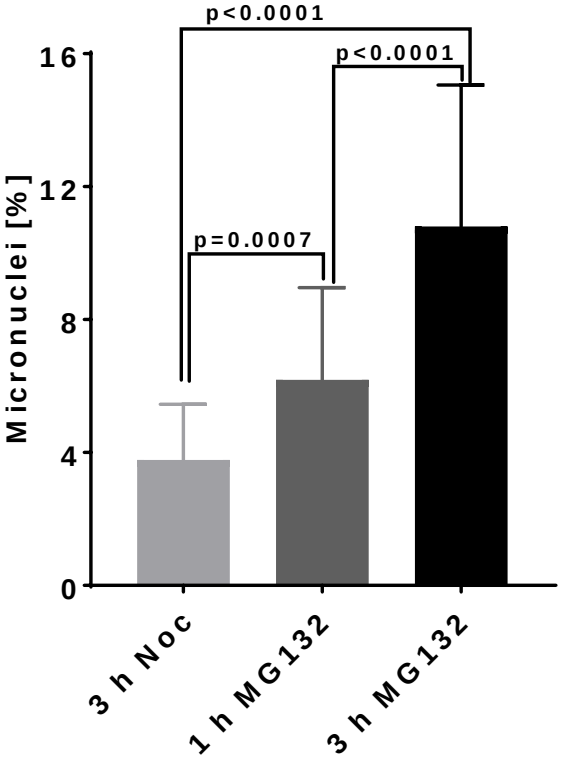

Figure_7

A

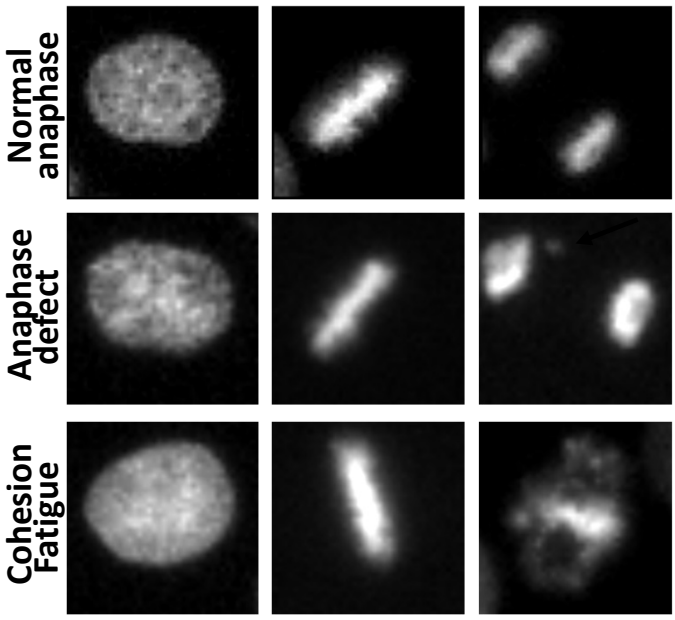
Normal anaphase
Anaphase defect
Cohesion Fatigue

B

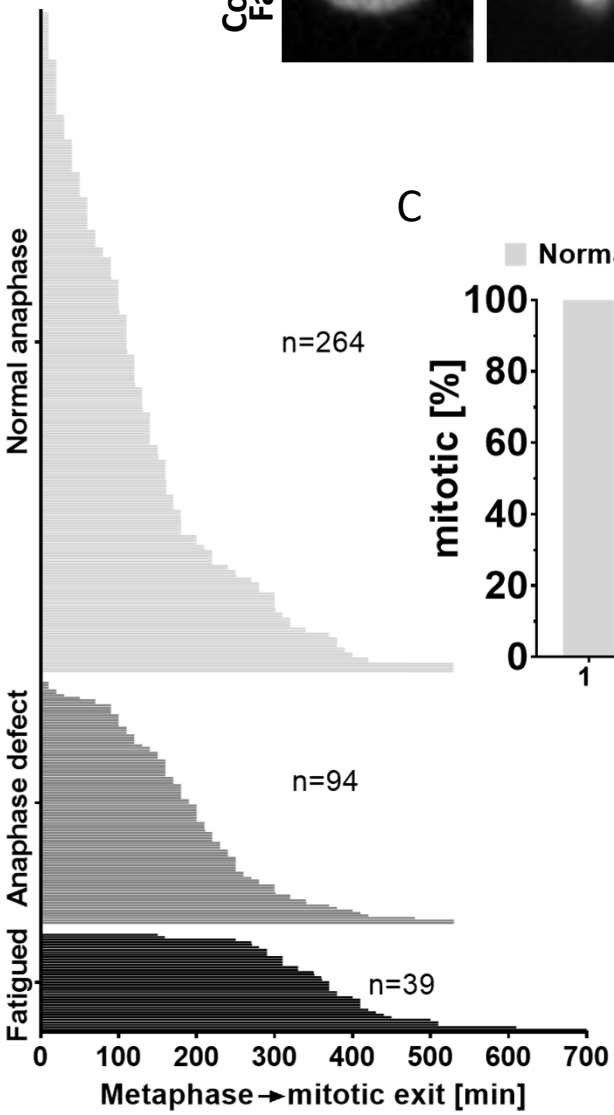
Normal anaphase
Anaphase defect
Fatigued
n=264
n=94
n=39
0
100
200
300
400
500
600
700
Metaphase→mitotic exit [min]

C

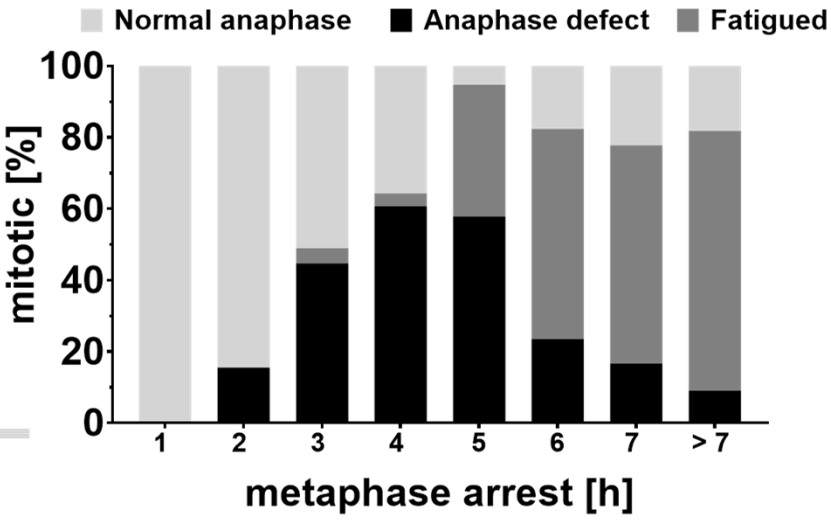
Normal anaphase
Anaphase defect
Fatigued
mitotic [%]
0
20
40
60
80
100
1
2
3
4
5
6
7
> 7
metaphase arrest [h]